Available online at www.sciencedirect.com
SCIENCE DIRECT®
Chemical Physics 301 (2004) 213–224
Chemical Physics
www.elsevier.com/locate/chemphys

Recoil velocity-dependent spin–orbit state distribution of chlorine photofragments

Lars Schäfer [a], Niels Gödecke [a], Oliver Ott [a], Christof Maul [a], Karl-Heinz Gericke [a,*], Peter S. Shternin [b], Elena V. Orlenko [b], Oleg S. Vasyutinskii [c]

[a] *Institut für Physikalische und Theoretische Chemie, Technische Universität Braunschweig, Hans-Sommer-Straße 10, D-38106 Braunschweig, Germany*
[b] *St. Petersburg Politechnical University, Politechnicheskaya 29, St. Petersburg 194021, Russia*
[c] *Ioffe Institute, Russian Academy of Sciences, Politechnicheskaya 26, St. Petersburg 194021, Russia*

Received 15 October 2003; accepted 11 December 2003
Available online 25 January 2004

Abstract

We present the results of experimental and theoretical studies of the speed-dependent spin–orbit state distributions of chlorine photofragments produced in the photodissociation of thiophosgene ($CSCl_2$) at 235 nm. Three-dimensional imaging has been employed for observing chlorine photofragments in their ground (Cl) and excited (Cl^*) spin–orbit states. The kinetic energy distributions for Cl and Cl^* fragments reflect excitation of several electronic states of the partner fragment CSCl. The spin–orbit branching ratio of $P(Cl^*)/[P(Cl) + P(Cl^*)]$ was found to depend on the kinetic recoil energy increasing from 0.1 for low kinetic energy to 0.8 for high kinetic energy.

The theoretical interpretation is based on the computation of the $CSCl_2$ potential energy surfaces (PES) along the C–Cl bond. Two completely different methods of determination of the PES were applied for small and for large values of the C–Cl bond separation R. In case of small and intermediate R values time-dependent density-functional theory has been used. In case of large R values we used an asymptotic method of computation of the PES, which is a generalisation of the Heitler–London approach for many-electron systems. Basis molecular wavefunctions with definite values of the total spin S and the spatial and spin reflection symmetry σ_v with respect to reflection of the total electronic wavefunction in the molecular plane were used. The developed theoretical approach was used for the assignment of the molecular states involved in the photodissociation and for the qualitative explanation of the non-statistical population of the spin–orbit states of the chlorine photofragments as function of the kinetic energy. The spin–orbit branching ratio of $P(Cl^*)/[P(Cl) + P(Cl^*)]$ predicted by the theory strongly depends on the quantum state of the CSCl fragment. It is large in case of the $CSCl(\tilde{X}) + Cl$ and $CSCl(\tilde{A}) + Cl$ channels and small in case of the $CSCl(\tilde{B}) + Cl$ channel which explains the experimental results.

1. Introduction

Photodissociation processes of polyatomic molecules that produce open shell atoms such as chlorine are widespread and have intensively been studied for decades because of their relevance for atmospheric chemistry (see, e.g. [1] and references therein). We will further denote such a molecule as RCl, where Cl is the chlorine atom and R is a polyatomic radical. There is essential complexity in understanding the underlying dynamics, because the photodissociation process usually involves several excited state surfaces. The first excited state of the chlorine atom is the $^2P_{1/2}$ state which lies only 882.4 cm^{-1} higher than the $^2P_{3/2}$ ground state. Therefore, the photodissociation of chlorine containing molecules generally produces a mixture of ground state $Cl(^2P_{3/2})$ atoms and spin–orbit excited $Cl^*(^2P_{1/2})$ atoms. Moreover, the quantum yield and the recoil anisotropy of Cl and Cl^* photofragments usually depend strongly on their velocity distribution [2–7].

These features have recently been investigated in the photodissociation of alkyl chlorides [2,3], phosgene ($COCl_2$) [4,6], thiophosgene ($CSCl_2$) [7], carbon tetrachloride (CCl_4) [5], nitrosyl chloride (ClNO) [5], thionyl

* Corresponding author. Fax: +49-531-391-5396.
E-mail address: k.gericke@tu-bs.de (K.-H. Gericke).

0301-0104/$ - see front matter © 2004 Elsevier B.V. All rights reserved.
doi:10.1016/j.chemphys.2003.12.012

chloride ($SOCl_2$) [5], and others. Many of these studies have given qualitatively similar results. For instance, in most cases the primary Cl^* atoms are: (1) less abundant than Cl atoms, (2) faster, and (3) more anisotropically distributed if there are no symmetry restrictions [5]. In spite of rapid recent developments of calculation methods the explanation of these features by direct ab initio methods is so far problematic. A three-state model based on Mulliken's treatment of alkyl halides [8] has been employed to interpret such results [5]. However, this simple model is not sufficient to understand the dissociation of more complex polyatomic molecules of reduced symmetry, especially if high lying excited electronic states might be involved.

The main idea of our paper is to develop a theoretical model which allows understanding of the general findings in the dissociation of polyatomic molecules containing chlorine atoms. We present experimental studies of the $CSCl_2$ photodissociation including the determination of the absorption spectrum of the parent thiophosgene molecule and the interpretation of our experimental results and of results reported elsewhere [7]. The theoretical interpretation is based on the computation of the $CSCl_2$ PES along the C–Cl bond. Two completely different methods for determining the PES were employed for small and for large values of the C–Cl bond separation R. For small and intermediate R values time-dependent density-functional theory (TDDFT) was used. Vertical excitation energies were provided along with state symmetries. Additionally, scans of excited state PES along one dissociating C–Cl bond in thiophosgene ($CSCl_2 + h\nu \rightarrow CSCl + Cl$) were performed within the Franck–Condon region in order to yield a deeper insight into the photodissociation process.

For large R values we used an asymptotic method of computation of the PES, which is a generalisation of the Heitler–London approach for many-electron molecular systems. Using basis molecular wavefunctions with definite values of the total spin S and the spatial and spin reflection symmetry σ_v with respect to reflection at the molecular plane, we diagonalised the Hamiltonian H and identified the molecular states involved in the photodissociation process. Note that the spatial and spin reflection symmetry σ_v coincides for singlet states with the conventional spatial C_s symmetry, but unlike C_s symmetry it remains a good symmetry when spin–orbit coupling is present. Particularly, it was shown that a non-statistical population of the spin–orbit chlorine states observed in the experiment can be explained by considering the transitions between molecular PES under the influence of strong non-adiabatic interactions and non-planarity at small recoil distances R. The spin–orbit branching ratio $P(Cl^*)/[P(Cl) + P(Cl^*)]$ predicted by the theory strongly depends on the quantum state of the CSCl fragment. It is large in case of the $CSCl(\tilde{X}) + Cl$ and $CSCl(\tilde{A}) + Cl$ channels and small in case of the $CSCl(\tilde{B}) + Cl$ channel which fits our experimental results. The developed theoretical model is general and can be used for interpretation of results in other polyatomic molecules containing chlorine atoms.

The organisation of the paper is as follows. In Section 2, we briefly present the results of previous studies of thiophosgene which are of relevance to the subject of the paper. Particularly, these are the geometry and the electron configuration of the ground and the lowest excited states of the molecule and details of the photolysis dynamics in the UV spectral range. In Section 3, we present the results of our experimental investigation of the thiophosgene photodissociation at 235 nm, including determination of the absorption spectrum and the speed distribution for ground state Cl and excited state Cl^* chlorine photofragments. Sections 4 and 5 present the main results of the theoretical interpretation of the experimental results. Section 4 contains a detailed explanation of our method of constructing the thiophosgene potential surfaces in the long range of the interfragment separation R for different dissociation channels, including different excited states of the molecular photofragment CSCl as well as the spin–orbit states of the atomic chlorine photofragments. Section 5 contains a qualitative analysis of the speed distributions of the chlorine photofragments and a comparison with experiment.

2. Thiophosgene molecule: previous studies

The structure and the gas phase photochemistry of thiophosgene have been the object of extensive study [9–15]. The structure of its ground state (X^1A_1) is shown in Fig. 1. Here and later we denote the quantum states of the parent $CSCl_2$ molecule by the capital letters without tilde, i.e., X, A, B, while the quantum states of the molecular fragment CSCl will be denoted by capital letters with tilde, i.e., $\tilde{X}$, $\tilde{A}$, $\tilde{B}$. The $CSCl_2$ molecule in the ground state is planar and belongs to the C_{2v} symmetry group. The electron configuration of the ground state has been determined by photoelectron spectroscopy to be [core] $(9a_1)^2(10a_1)^2(6b_2)^2(11a_1)^2(7b_2)^2(3b_1)^2(12a_1)^2(2a_2)^2(13a_1)^2(8b_2)^2(4b_1)^2(9b_2)^2$, where the $11a_1$, $7b_2$, and

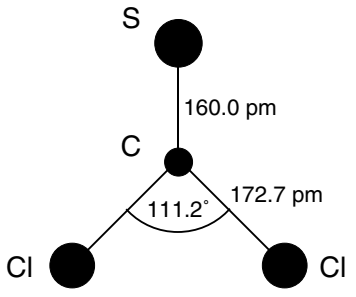

Fig. 1. Equilibrium geometry of the planar thiophosgene $CSCl_2(X^1A_1)$ ground state. Values are taken from the microwave study of [15].

$12a_1$ molecular orbitals (MOs) contain the σ bonding electrons, the $3b_1$ and $4b_1$ MOs contain the π bonding electrons and the Cl(3pπ) lone pair which strongly mix with each other, and the $2a_2$, $13a_1$, $8b_2$, and $9b_2$ MOs contain the remaining chlorine and the sulphur lone pair electrons all of which are essentially non-bonding [16].

The low excited states of thiophosgene have been studied by optical absorption/fluorescence spectroscopy and by electron impact energy loss spectroscopy. The weak absorption in the visible has been assigned to the excitation of the first singlet excited state A ($A^1A_2 \leftarrow X^1A_1$), which corresponds to a dipole-forbidden $\pi^* \leftarrow n$ ($5b_1 \leftarrow 9b_2$) electron promotion and is accompanied by the corresponding $a^3A_2 \leftarrow X^1A_1$ singlet–triplet excitation at somewhat longer wavelengths. This excitation is very well understood. Absorption in the strong band system in the near-UV region populates the second excited singlet state, B, which mainly arises from the promotion of a $4b_1$ electron to the $5b_1$ MO. The $\pi^* \leftarrow \pi$, $B(^1A_1) \leftarrow X(^1A_1)$ transition results in lowering the C–S bond order, lengthening the C–S bond by about 0.5 Å and decreasing the Cl–Cl bond angle from 111.2° to 103° [15,17]. Farnworth's and King's analysis [10] of the absorption bands between 250 and 290 nm indicated that the B state has a pyramidal structure with an equilibrium out-of-plane angle of about 20° and an inversion barrier of about 126 cm^{-1}. Below 257 nm no vibrational structure in absorption and no fluorescence could be recorded. Excitation of the molecule in this spectral region results mainly in fast photodissociation to CSCl + Cl as indicated by Okabe [11] and shown in direct experiments by Ondrey and Bersohn [13] at 248 nm and by Einfeld et al. [7] at 235 nm.

The $B(^1A_1) \leftarrow X(^1A_1)$ transition bears several intriguing features which made it the subject of a large number of theoretical as well as experimental studies [18]. First, the spectrum is very complex and consequently difficult to analyse because of the drastic geometrical change of the molecule upon excitation. Second, fluorescence from the second excited singlet state is unusual in principle. Third and most important, experimental evidence was found for another dark state in the vicinity of the $B(^1A_1)$ state, the nature of which has still not been identified beyond doubt [18].

As far as photochemistry is concerned, ab initio calculations of the vertical excitation energies of the 10 lowest electronic states of the CSCl radical performed by Hachey et al. [14] have shown that the electronic ground state and two low-lying excited doublet states of CSCl, $\tilde{X}$, $\tilde{A}$, and $\tilde{B}$, are accessible in the UV photolysis of $CSCl_2$.

This prediction has recently been employed by Einfeld et al. [7] who determined the relative yield of these three electronic states in $CSCl_2$ photodissociation at 235 nm for each of the Cl and Cl^* channels together with the speed distributions for both spin–orbit states and the respective anisotropy parameters β. The relative yields were found to be: $P_{Cl}(\tilde{X}):P_{Cl}(\tilde{A}):P_{Cl}(\tilde{B}) = 2:32:19$ and $P_{Cl^*}(\tilde{X}):P_{Cl^*}(\tilde{A}):P_{Cl^*}(\tilde{B}) = 3.5:33.5:10$. Thus, the fast chlorine fragments correlating with the $CSCl(\tilde{X})$ channel are mostly produced in their spin–orbit excited state $^2P_{1/2}$, while the slow chlorine fragments correlating with the $CSCl(\tilde{B})$ channel are mostly produced in their ground state $^2P_{3/2}$. The Cl fragments at intermediate speeds correlating with the $CSCl(\tilde{A})$ channel have their spin–orbit states populated approximately equally. This result is illustrated by Fig. 2 where the relative number of the Cl^* atoms depends dramatically on the fragment recoil velocity varying from 0.1 for low speeds to 0.8 for high speeds.

Each of the CSCl quantum states $\tilde{X}$, $\tilde{A}$, and $\tilde{B}$ has a singly occupied orbital of either σ or π character. The vertical excitation energy calculation of the CSCl radical [14] yielded the following configurations and vertical excitation energies of the quantum states:

$$\tilde{X}:\ (1a')^2(1a'')^2\cdots(15a')^2(4a'')^2 16a',\quad E(\tilde{X}) = 0,$$

$$\tilde{A}:\ (1a')^2(1a'')^2\cdots(15a')^2(4a'')^2 5a'',\quad E(\tilde{A}) = 1.58\ \text{eV},$$

$$\tilde{B}:\ (1a')^2(1a'')^2\ldots(14a')^2(4a'')^2 15a'(16a')^2,$$
$$E(\tilde{B}) = 3.14\ \text{eV}.$$

Therefore, the singly occupied orbital in the ground state $\tilde{X}$ is of a′ symmetry having the main character of a σ(C) atomic orbital. The singly occupied orbital of the first excited state $\tilde{A}$ is of a″ symmetry having π*(C–S) main character. Finally, the singly occupied orbital of the second excited state $\tilde{B}$ is of a′ symmetry having σ(S) main character.

The MRSD-CI geometry optimisation of the ground state and the lowest excited state of CSCl has been done in [14] and led to the following result. $\tilde{X}^2A'$ state:

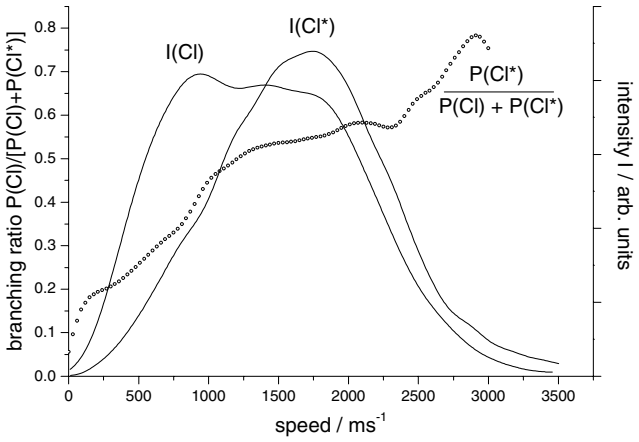

Fig. 2. Velocity-dependent spin–orbit state distributions of Cl photofragments produced in the photodissociation of thiophosgene at 235 nm. Circles show the branching ratio obtained from the spin–orbit state-specific speed distributions which are shown by solid lines.

$R_{CS}^{X} = 158.0$ pm, $R_{CCl}^{X} = 168.8$ pm, and $\alpha^{X}(CSCl) = 134.1°$. $\tilde{A}^2A''$ state: $R_{CS}^{A} = 158.8$ pm, $R_{CCl}^{A} = 165.1$ pm, and $\alpha^{A} = 180°$. Therefore, the lowest excited state $\tilde{A}^2A''$ is expected to be linear.

3. Experiment

The absorption spectrum of thiophosgene (purity 97%) was measured in the range from 650 to 200 nm at room temperature for a vapour sample using a commercially available UV/VIS/NIR spectrometer (Perkin–Elmer, Lambda 900). A quartz absorption cell with an optical path length of 10 cm was evacuated and purged with thiophosgene several times. The measurement was carried out at a pressure of 137 mbar in the visible spectral range and at 1.13 mbar in the UV spectral range. Pressures were determined by a differential capacitance gauge (MKS, Baratron 221). The observed absorption spectrum is shown in Fig. 3. Well-known structured absorption between 560 and 390 nm was observed and several overlapping absorption bands in the range below 280 nm were found [19]. To our knowledge the data below 240 nm are reported for the first time.

The photodissociation dynamics of thiophosgene ($CSCl_2$) at a wavelength around 235 nm were studied by three-dimensional imaging employing resonance enhanced multi-photon ionisation (REMPI) in an apparatus consisting of a single-field time-of-flight (TOF) mass spectrometer and a position-sensitive detector (PSD). The experimental set-up is described in detail elsewhere [6,20,21]. The apparatus was evacuated to a base pressure of ca. 10^{-7} mbar. Thiophosgene was seeded in argon as buffer gas and fed into the spectrometer via a continuous supersonic molecular beam. By cooling thiophosgene to −15 °C the concentration of the prepared mixture was ca. 0.5% $CSCl_2$ in argon. The temperature of the molecules under the given conditions (nozzle diameter 20 μm, stagnation pressure ~1.5 bar, working pressure $\sim 10^{-6}$ mbar) is about 8 K, determined by a rotationally resolved calibration spectrum of the $V^1\Sigma^+(v' = 12, J') \leftarrow X^1\Sigma^+(v = 0, J)$ transitions of HCl. The dissociation and state-selective detection of chlorine atoms were performed in a one-colour experiment using the second harmonic of a dye laser (Lambda Physik, Scanmate) pumped by the third harmonic of a Nd:YAG laser (Coherent, Infinity 40–100). The polarisation of the frequency-doubled light could be changed by a half-wave plate. A 200-mm lens was used to decrease the reaction volume to 5×10^{-4} mm^3. In order to prevent transfer of kinetic energy to the fragments due to space charge effects and saturation of the dissociation step the energy per pulse was carefully adjusted to an amount of ca. 50 μJ. To verify the desired perpendicular overlap between laser beam and molecular beam HCl was monitored by REMPI at 235.99 nm at regular intervals. In the $CSCl_2$ photodissociation experiments, the (2 + 1)-REMPI process yields chlorine ions from ground state $Cl(^2P_{3/2})$ and excited state $Cl^*(^2P_{1/2})$ fragments, which were accelerated by a voltage of typically 450 V, corresponding to a field of 9 kV/m. Chlorine atoms in the ground state were state-selective probed via the $(^2D_{3/2} \leftarrow {}^2P_{3/2})$ transition at 235.336 nm. The excited state, which lies 882.4 cm^{-1} above the ground state due to spin–orbit coupling, was probed by the $(^2P_{1/2} \leftarrow {}^2P_{1/2})$ transition at 235.205 nm. By scanning the dye laser over a range of ±0.003 nm around the centres of the transitions the Doppler broadening was taken into account. Signals from the PSD, digitised by time-to-digital converters, were saved to a personal computer. Measuring both the position of every individual particle on the detector and its TOF, we determined the full three-dimensional velocity distribution and extracted the complete information about the kinetic energy distribution and the velocity-dependent anisotropy parameter β.

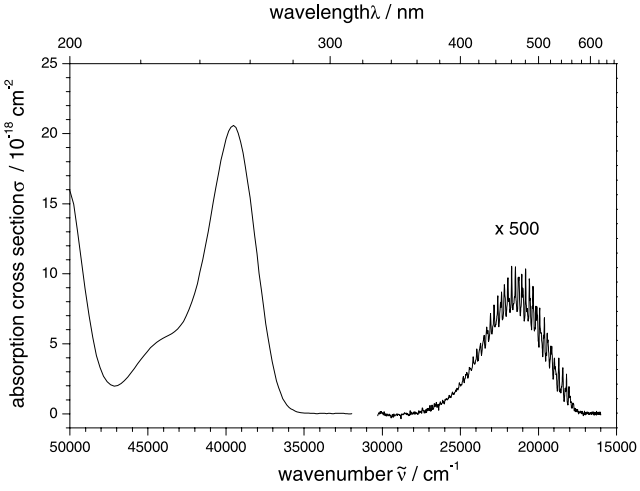

Fig. 3. Absorption spectrum of the $CSCl_2$ molecule.

In the case of thiophosgene the determined value of the β parameter both for Cl and Cl* is close to zero in the whole recoil velocity range. The speed dependence of the branching ratio as well as the kinetic energy distributions for chlorine atoms in the ground and excited states are shown in Fig. 2.

4. Vertical excitation energies and potential energy surfaces

We consider the interaction between a Cl atom in its ground state configuration $3p^5$ and a doublet radical R in the quantum state described by a wavefunction of $^2\sigma$ or $^2\pi$ character. The complexity of constructing PES for this system and of understanding the underlying photodissociation dynamics is due to a large number of

molecular excited state surfaces, which are involved in the photodissociation process, and due to multiple interatomic interactions, which occur between the photofragments. Particularly, the Cl atom in its ground state configuration can exist in six different $j\Omega_j$ ($j = 1/2,\ 3/2$) quantum states. Therefore, the total number of molecular states is 12 in the $Cl + R(\sigma)$ channel and is 24 in the $Cl + R(\pi)$ channel. In order to consider the $P(Cl^*)/[P(Cl) + P(Cl^*)]$ branching ratio the spin–orbit interaction in the chlorine atom fragment must be taken into account simultaneously with the intermolecular interactions which complicates the problem. However, as we will show in this paper an appropriate representation of the molecular wavefunctions can greatly reduce the number of states under consideration and gives a simple predictive model of the photodissociation process.

Assuming the photodissociation process to be fast compared to the time of molecular rotation, we construct a one-dimensional correlation diagram of the planar $CSCl_2$ molecule and its separated dissociation fragments, starting from the equilibrium geometry of C_{2v} symmetry in Fig. 1 and increasing the length of one dissociating C–Cl bond which transforms the molecular geometry to C_s symmetry.

Note that in fact the excited states of the $CSCl_2$ molecule are apparently not planar, but have a pyramidal structure [10]. However, the planar model above is useful because it allows to correlate the results of TDDFT calculations of the PES for the Franck–Condon region to the results of the Heitler–London type approximation calculations for the asymptotic region (see below). Also, using the reflection symmetry σ_v reduces the number of the molecular wavefunctions which should be considered simultaneously in the asymptotic region by a factor of 2. In this representation the out-of-plane equilibrium geometry of the molecular excited states leads to transitions between the excited potential surfaces of a′ and a″ symmetry occurring during the dissociation process, which can be taken into consideration by introducing phenomenological transition probabilities.

4.1. Vertical excitation energies and oscillator strengths

The ground and electronically excited states of $CSCl_2$ for small and intermediate values of the distance R between the photofragments have been computed using time-dependent density-functional theory [22] based on the hybrid functional B3LYP [23]. Vertical excitation energies are provided along with state symmetries. Additionally, excited state potential surface scans along one dissociating C–Cl bond in thiophosgene ($CSCl_2 + h\nu \rightarrow CSCl + Cl$) have been performed for small and intermediate values of R. All calculations have been carried out using the Gaussian 98 program package [24] using the 6-311+G(3df) basis set.

Vertical excitation energies and the corresponding oscillator strengths along with electronically excited state symmetries are given in Table 1. The arrows in the first column indicate the correlation between the irreducible representations of the equilibrium C_{2v} geometry of the molecule and the C_s non-equal C–Cl bonds geometry arising due to the molecular dissociation. The $CSCl_2$ ionisation threshold was calculated to be 7.3 eV. According to Casida et al. [25], an excitation has to fulfil the following criteria in order to be correctly described by TDDFT. First, the excitation energy should be significantly smaller than the ionisation energy. Second, the excitation should not involve major contributions from promotions to virtual orbitals which are only weakly bound or even unbound in the selected functional. Thus, excitations to energetically low lying states are usually described reasonably well by TDDFT, also in the case of thiophosgene. Both criteria are fulfilled quite well for the lower $CSCl_2$ excited states, but become more and more violated for the higher states.

The relationship between excited states of thiophosgene shown in Table 1 and those known from previous studies (see, e.g. [18]) is most likely as follows: $1^3A_2 \Longleftrightarrow a^3A_2$, $1^3A_1 \Longleftrightarrow b^3A_1$, $1^1A_2 \Longleftrightarrow A^1A_2$, $2^1A_1 \Longleftrightarrow B^1A_1$, and $1^1B_2 \Longleftrightarrow C^1B_2$. Note that excitations from the $^1A_1$ ground state to $^1A_2$ excited states are dipole-forbidden within the framework of C_{2v} symmetry. Singlet–triplet transitions are also forbidden.

According to Table 1 only two excited molecular states, namely 2^1A_1 and 1^1B_2, can contribute to optical

Table 1
Planar ground state (equilibrium) geometry: calculated $CSCl_2$ vertical excitation energies (TD-B3LYP/6-311+G(3df))[a]

	ΔE (eV)	Oscillator strength
$CSCl_2$ singlet electronic state[b]		
$1^1A_2 \rightarrow 1^1A''$ (A)	2.72	0.0000
$2^1A_2 \rightarrow 2^1A''$	4.88	0.0000
$2^1A_1 \rightarrow 2^1A'$ (B)	4.92	0.1053
$1^1B_2 \rightarrow 3^1A'$ (C)	5.03	0.0034
$1^1B_1 \rightarrow 3^1A''$	5.51	0.0009
$2^1B_2 \rightarrow 4^1A'$	5.76	0.0614
$2^1B_1 \rightarrow 4^1A''$	6.02	0.0000
$3^1B_2 \rightarrow 5^1A'$	6.40	0.0411
$3^1A_1 \rightarrow 6^1A'$	6.73	0.3349
$CSCl_2$ triplet electronic state[b]		
$1^3A_2 \rightarrow 1^3A''$ (a)	2.25	
$1^3A_1 \rightarrow 1^3A'$ (b)	2.78	
$1^3B_2 \rightarrow 2^3A'$	4.64	
$2^3A_2 \rightarrow 2^3A''$	4.73	
$2^3B_2 \rightarrow 3^3A'$	5.07	
$1^3B_1 \rightarrow 3^3A''$	5.19	
$2^3B_1 \rightarrow 4^3A''$	5.61	
$2^3A_1 \rightarrow 4^3A'$	5.82	

[a] Ground state optimised at UB3LYP/6-311+G(3df) level of theory.
[b] C_s symbols refer to a planar ground state with one elongated C–Cl bond (see Table 3). Commonly employed state labels are given in parentheses.

excitation from the 1^1A_1 ground state of thiophosgene molecule at 235 nm. In view of the accuracy of TDDFT, a possible participation of the 1^1B_1 and the 2^1B_2 states need also to be considered. The data shown in Table 1 have been calculated assuming the planar equilibrium geometry of the molecular ground state of C_{2v} ($^1A_1$) symmetry which is shown in Fig. 1. However, vertical excitation from a non-equilibrium geometry of the molecular ground state can also be important. To explore this possibility we computed the vertical excitation energies for two non-equilibrium configurations of the thiophosgene ground state.

Results of this calculation for the pyramidal $1^1A'$ ground state geometry with out-of-plane angle of 10° are shown for singlet excited states in Table 2. Note that the symmetry reflection label (A' or A'') of the same excited states in Tables 1 and 2 is not always the same, because the plane of reflection in Table 1 is perpendicular to the plane of reflection in Table 2. As seen from the comparison between Tables 1 and 2 the pyramidal geometry of the ground state does not change the oscillator strengths or the vertical excitation energies dramatically. However, the oscillator strengths for the $3^1A''$ (1^1B_2) and $3^1A'$ (1^1B_1) states in Table 2 become comparable to each other, and therefore, the four $2^1A'$ (2^1A_1), $3^1A''$ (1^1B_2), $3^1A'$ (1^1B_1), and $4^1A''$ (2^1B_2) excited states need to be considered to contribute to the absorption at 235 nm.

The result of the calculations for the asymmetric C–Cl stretching mode planar ground state geometry is shown for singlet excited states in Table 3. In this case the order of the states is changed, but the states $2^1A'$ (2^1A_1) and $3^1A'$ (1^1B_2) are still likely to give the major contribution to the absorption intensity at 235 nm.

4.2. Calculation of the potential energy surfaces

The interaction between the Cl atom and the CSCl fragment and the corresponding electron wavefunctions can be represented in different forms depending on the distance R between the centres of mass of the photo-fragments (see, e.g. [26]). Later, we use the body-fixed frame XYZ with the Z-axis parallel to R and the Y-axis perpendicular to the molecular plane. The free-fragment states (FFS) at $R \to \infty$ can be represented as a product of the free fragment wavefunctions in the body-fixed frame. These wavefunctions are the zero-order eigenfunctions of the molecular electronic Hamiltonian H_{el} for the distances R, where the interfragment interaction ΔV_{mol} is smaller than the spin–orbit interaction ΔV_{SO}. For these states good quantum numbers are those of total angular momentum of the Cl atom j, the modulus of the projection $|\Omega_j|$ of j onto the Z-axis, the internal electronic state $\tilde{N}$ of the CSCl fragment, [1] and σ_v, where $\sigma_v = \pm 1$ is the reflection symmetry of the total electronic molecular wavefunction with respect to reflection of spatial and spin coordinates of all electrons in the molecular plane XZ.

The weakly perturbed states (WPS) are those whose wavefunctions are the zero-order eigenfunctions of H_{el} for the R distances where the intermolecular interaction ΔV_{mol} is larger than the spin–orbit interaction ΔV_{SO}, but still smaller than the energy intervals $\Delta V_{frag} = E(\tilde{B}) - E(\tilde{A})$, $E(\tilde{A}) - E(\tilde{X})$ between the electronic states of the molecular fragment: $\Delta V_{SO} < \Delta V_{mol} < \Delta V_{frag}$. For these states good quantum numbers are those of the orbital angular momentum of the Cl atom L, ($L = 1$), $\tilde{N}$, σ_v, and S, where S is the total spin of the $CSCl_2$ molecule.

Finally, the strongly perturbed states (SPS) are those which are relevant for small R distances, including the Franck–Condon region where $\Delta V_{SO} < \Delta V_{frag} < \Delta V_{mol}$. Good quantum numbers for this region are S and σ_v.

Two different methods have been used for constructing the one-dimensional molecular PES for SPS and WPS–FFS regions.

Table 2
Pyramidal ground state geometry

$CSCl_2$ electronic state[a]	ΔE (eV)	Oscillator strength
$1^1A''$ (1^1A_2)	2.70	0.0001
$2^1A''$ (2^1A_2)	4.81	0.0000
$2^1A'$ (2^1A_1)	4.87	0.1011
$3^1A''$ (1^1B_2)	5.06	0.0026
$3^1A'$ (1^1B_1)	5.49	0.0031
$4^1A''$ (2^1B_2)	5.72	0.0618
$4^1A'$ (2^1B_1)	6.05	0.0001
$5^1A''$ (3^1B_2)	6.42	0.0415

Calculated $CSCl_2$ singlet-state vertical excitation energies (TD-B3LYP/6-311+G(3df)).

[a] C_{2v} symbols in parentheses refer to Table 1.

Table 3
Asymmetric C–Cl stretching mode/planar geometry: calculated $CSCl_2$ singlet state vertical excitation energies (TD-B3LYP/6-311+G(3df))

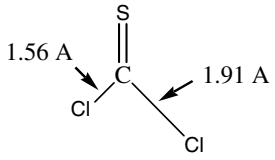

$CSCl_2$ electronic state[a]	ΔE (eV)	Oscillator strength
$1^1A''$ (1^1A_2)	2.75	0.0000
$3^1A'$ (1^1B_2)	4.31	0.0053
$2^1A''$ (2^1A_2)	4.73	0.0000
$2^1A'$ (2^1A_1)	5.19	0.1286
$3^1A''$ (1^1B_1)	5.32	0.0001
$4^1A''$ (2^1B_1)	5.40	0.0008
$4^1A'$ (2^1B_1)	5.57	0.1314
$5^1A''$ (3^1B_2)	6.05	0.0394

[a] C_{2v} symbols in parentheses refer to Table 1.

[1] Here and later we neglect the spin–orbit interaction in the CSCl molecular fragment.

4.2.1. SPS region

The PES in the SPS region have been obtained in two steps: First, the geometry at each point on the PES was optimised along a C–Cl bond at the UHF/6-311+G(d) level for the ground state. Second, single-point energy calculations at each optimised geometry of the ground state were performed at the TD-UB3LYP/6-311+G(d) level of theory for prediction of the excited singlet states. The zero energy was taken to be the minimum of the ground state PES.

4.2.2. WPS–FFS region

The PES in the WPS–FFS region have been calculated by an asymptotic method which is a generalisation of the Heitler–London approach for a many-electron molecular system [27]. The effective electronic molecular Hamiltonian H_{eff} can be presented as

$$H_{\text{eff}} = H_{\text{orb}} + V_{\text{SO}} + V_{\text{C}}, \tag{1}$$

where H_{orb} and V_{SO} are the pure orbital and spin–orbital Hamiltonians, respectively, while the term V_{C} represents the long-range Coulomb (multipole) interaction between the fragments.

Five equivalent valence p electrons of the Cl atom and one singly occupied atomic p orbital of the CSCl fragment of the σ, or π character have been taken into consideration in the electron orbital operator H_{orb} in Eq. (1) which was used in the following form:

$$H_{\text{orb}} = \sum_{i=1}^{6}\left(-\frac{1}{2}\Delta_i - \frac{5}{|\mathbf{r}_i - \mathbf{R}|} - \frac{1}{r_i}\right) + \sum_{i=1}^{6}\sum_{k>i}^{6}\frac{1}{|\mathbf{r}_i - \mathbf{r}_k|} + \frac{5}{R}, \tag{2}$$

where $\mathbf{r}_i$ and Δ_i are the radius vector and the kinetic energy operator of the ith electron, and R is the inter-fragment distance. The origin in Eq. (2) is on the centre of the quasi-atomic singly occupied orbital of either σ, or π character in the CSCl fragment. This orbital can be associated with the unpaired molecular orbital centred on either the C or the S atom, or even on the C–S bond (see discussion in the end of Section 2).

The model is approximately restricted to large R values where the intermolecular interaction ΔV_{mol} is smaller than the energy intervals between the electronic states of the molecular fragment ΔV_{frag}. However, the exact region of validity of the model can be determined only by comparing with the results of full quantum chemical calculations.

When electron 1 belongs to the molecular fragment and electron 2 is one of the five equivalent electrons of the Cl atom, the operator H_{orb} in Eq. (2) can be represented as $H_{\text{orb}} = H_0 + H_{\text{int}}$, where

$$H_0 = \sum_{i=3}^{6}\left(-\frac{1}{2}\Delta_i - \frac{5}{|\mathbf{r}_i - \mathbf{R}|}\right) + \sum_{i=3}^{6}\sum_{k>i}^{6}\frac{1}{|\mathbf{r}_i - \mathbf{r}_k|}, \tag{3}$$

$$H_{\text{int}} = \sum_{i=1}^{2}\left(-\frac{1}{2}\Delta_i - \frac{5}{|\mathbf{r}_i - \mathbf{R}|}\right) + \sum_{i=1}^{6}\frac{1}{r_i} + \sum_{i=1}^{2}\sum_{k>i}^{6}\frac{1}{|\mathbf{r}_i - \mathbf{r}_k|} + \frac{5}{R}. \tag{4}$$

The operator H_0 in Eq. (3) is the Hamiltonian of the fragment ionic cores and the term H_{int} in Eq. (4) represents interaction of the electrons 1 and 2 with both cores, between each other, and interaction between the cores. Separation of the operator H_{orb} in two parts, H_0 and H_{int}, is useful because the operator H_0 matrix elements result only in a global shift of all PES and therefore need not be calculated explicitly.

Only spin–orbit interaction in the chlorine atom has been taken into consideration in the operator V_{SO}.

The operator V_{C} in Eq. (1) contains contributions from the two leading terms of the multipole expansion: the dipole–quadrupole (DQ) and the quadrupole–quadrupole (QQ) interaction between the photofragments, $V_{\text{C}} = V_{\text{DQ}} + V_{\text{QQ}}$ [28]:

$$V_{\text{DQ}} = \frac{6}{R^4}\sum_{q=-1}^{1}\frac{1}{[(1-q)!(1+q)!(2-q)!(2+q)!]^{1/2}} \times Q^1_{q\text{M}}Q^2_{-q\text{A}}, \tag{5}$$

$$V_{\text{QQ}} = \frac{24}{R^5}\sum_{q=-2}^{2}\frac{1}{(2-q)!(2+q)!}Q^2_{q\text{M}}Q^2_{-q\text{A}}, \tag{6}$$

where $Q^{K_{\text{A}}}_{q\text{A}}$ and $Q^{K_{\text{M}}}_{q\text{M}}$ are spherical components of the corresponding multipole operators for the molecular (M) and the atomic (A) fragment, respectively. They are given by the expression

$$Q^K_q = \sum_i q_i r_i^K \sqrt{\frac{4\pi}{2K+1}}Y_{Kq}(\theta_i, \varphi_i), \tag{7}$$

where q_i, r_i, θ_i, and φ_i are the charge and spherical coordinates of the ith particle (electronic or nuclear), where the Z-axis is parallel to the vector $\mathbf{R}$, the origin is in the centre of mass of the corresponding fragment, and $Y_{Kq}(\theta_i, \varphi_i)$ is a spherical harmonic. The summation in Eq. (7) runs over all charged particles of the fragment.

Calculating the Hamiltonian H_{eff} matrix elements in Eq. (1), we used a basis set of molecular wavefunctions with definite values of the total molecular spin S and reflection symmetry σ_{v} with respect to reflection of the *spatial and spin coordinates* of the electrons at the molecular plane. These wavefunctions were those related to the WPS region and can be presented in the following general form,

$$\Psi_{\mathrm{mol}} = \frac{1}{t_\lambda}(|L_\mathrm{A}\Omega_\mathrm{A}, \Omega_\mathrm{M}, S\mu\rangle \pm |L_\mathrm{A} - \Omega_\mathrm{A}, -\Omega_\mathrm{M}, S-\mu\rangle), \tag{8}$$

where L_A and Ω_A are the orbital angular momentum of the atomic fragment and its projection onto the Z-axis, Ω_M is the angular momentum projection of the unpaired p orbital of the molecular fragment, and S and μ are the total electronic spin of the molecule and its projection. The normalisation factor t_λ in Eq. (8) is equal to $t_\lambda = \sqrt{2}$ in case of $\lambda \neq 0$ and $t_\lambda = 2$ in case of $\lambda = 0$, where $\lambda = |\Omega_\mathrm{A} + \Omega_\mathrm{M} + \mu|$. The wavefunctions $|L_\mathrm{A}\Omega_\mathrm{A}, \Omega_\mathrm{M}, S\mu\rangle$ in Eq. (8) are transformed under reflection in the molecular frame σ_v as

$$\hat{\sigma}_\mathrm{v}|L_\mathrm{A}\Omega_\mathrm{A}, \Omega_\mathrm{M}, S\mu\rangle = p_\mathrm{A}p_\mathrm{M}(-1)^{S-\mu+L_\mathrm{A}-\Omega_\mathrm{A}+L_\mathrm{M}-\Omega_\mathrm{M}} \times |L_\mathrm{A} - \Omega_\mathrm{A}, -\Omega_\mathrm{M}, S-\mu\rangle, \tag{9}$$

where $p_\mathrm{A} = -1$ and $p_\mathrm{M} = -1$ are the parities of the atomic and molecular fragments A and M, respectively, and $L_\mathrm{A} = L_\mathrm{M} = 1$.

Later, we introduce the group symmetry label $(^{2S+1}\mathrm{A})'/(^{2S+1}\mathrm{A})''$, where $S = 0, 1$, denoting the molecular states which are associated with the *spatial and spin* symmetry index $\sigma_\mathrm{v} = +1/-1$, respectively. For singlet molecular states this label is equivalent to the conventional C_s point group symmetry label $^1\mathrm{A}'/^1\mathrm{A}''$ which is associated with reflection of the *spatial* electron coordinates only, e.g., $(^1\mathrm{A})' \equiv {}^1\mathrm{A}'$ and $(^1\mathrm{A})'' \equiv {}^1\mathrm{A}''$. However, in the whole WPS–FFS region we will use the symmetry labels $(^{2S+1}\mathrm{A})'/(^{2S+1}\mathrm{A})''$ because the conventional C_s point group symmetry labels are mixed by the spin–orbit interaction.

The interaction operator H_int, which dominates in the region $R \leqslant 3$ Å, is diagonal in the representation (8) over the quantum numbers S and μ. Thus, simple assignment of the singlet and triplet quantum states is possible in this region as well as their matching with the molecular states computed for the SPS region. The spin–orbit interaction operator V_SO and the long-range Coulomb operator V_C are in general non-diagonal in the representation (8) over the quantum numbers S and μ, however, they do not mix the molecular wavefunctions with opposite reflection indices σ_v. Therefore, within the planar molecular geometry the basis set in Eq. (8) in the whole range of R values is divided in two non-interacting groups of molecular wavefunctions with respect to reflection in the molecular plane.

Taking into account the indistinguishability of all six electrons the multi-electron matrix elements of the operators H_int and V_SO over the wavefunctions from Eq. (8) were presented as sums containing one- and two-electron matrix elements. These matrix elements have been evaluated following the method given in [27,29] with the program Maple 8 over the asymptotic one-electron atomic wavefunctions [30],

$$\psi_i = Cr_i^{(1/\alpha)-1}\,\mathrm{e}^{-\alpha r_i} \quad \text{with } \alpha = \sqrt{2I}, \tag{10}$$

where I is the atomic ionisation potential of either the Cl or the C or the S atom.

The matrix elements of the long-range Coulomb interaction operator V_C have been calculated directly using the WPS molecular wavefunctions basis (8) and the Wigner–Eckart theorem [31]. The quadrupole moment of the Cl atomic fragment $Q_\mathrm{Cl} \approx 1.47D$ Å has been calculated following the method given in [32]. The components of the dipole and quadrupole moments of the CSCl fragment were calculated using the standard DFT method. These components related to the electronic ground state $\tilde{\mathrm{X}}$ of the fragment are shown in Tables 4 and 5. They were used for determining the values of the reduced matrix elements of the dipole–quadrupole and quadrupole–quadrupole interactions. The values of the components for the excited $\tilde{\mathrm{A}}$ and $\tilde{\mathrm{B}}$ fragment states are similar to that for the $\tilde{\mathrm{X}}$ state in Tables 4 and 5. Our calculations have shown that the contribution from the matrix elements of the operator V_C to the resulting PES below can be neglected compared with the contribution from the operators H_int and V_SO.

The advantage of the basis set in Eq. (8) is that it allows to group the quantum states according to their multiplicity which greatly simplifies the analysis. For instance, the total number of molecular states in the Cl + R(σ) channel is 12, however, six states of $(\mathrm{A})'$ symmetry and six states of $(\mathrm{A})''$ symmetry can be considered separately from each other. Moreover, only *three* of them are singlet in the WPS region: *two* of $(^1\mathrm{A})'$ symmetry and *one* of $(^1\mathrm{A})''$ symmetry. These states can most likely be populated by optical excitation of the parent molecule and they are mostly important for the following analysis.

Two 6×6 matrices which correspond to the effective electron molecular Hamiltonian H_eff for the Cl + R(σ) channel have been diagonalised using the program Maple 8 providing the PES for the whole WPS–FFS region. The

Table 4
Components of the dipole moment of the CSCl radical

$M_{X'}$ (Debye)	$M_{Z'}$ (Debye)
0.2216	0.0275

Table 5
Components of the quadrupole moment of the CSCl radical

$Q_{X'X'}$ (Debye Å)	$Q_{Y'Y'}$ (Debye Å)	$Q_{Z'Z'}$ (Debye Å)	$Q_{X'Z'}$ (Debye Å)
−0.9910	−0.1452	1.1362	1.1825

$X'Y'Z'$ frame: CSCl molecule is in the $X'Z'$ plane, SC is in the negative part of the Z'-axis, C is in the origin, Cl is in the positive $X'Z'$ quarter. The ground state was optimised at UB3LYP/6-311+G(3df) level of theory to be $R_\mathrm{CS} = 157.02$ pm, $R_\mathrm{CCl} = 169.33$ pm, and $\alpha(\mathrm{SCCl}) = 135.51°$.

resultant PES of $(A)'$ and $(A)''$ symmetry calculated for the $Cl + R(\tilde{X})$ channel are shown in Figs. 4 and 5, respectively. As mentioned in Section 2, in this case the bonding σ orbital of the CSCl fragment is mainly localised on the carbon atom [14]. Similar PES were obtained for the $Cl + R(\tilde{B})$ case when the orbital is mainly localised on the sulphur atom [14]. One can see from Fig. 4 that one of the possible $(^1A)'$ states in the WPS region adiabatically correlates with the lower spin–orbit state of Cl atom at large R values, while the other $(^1A)'$ state adiabatically correlates with the upper spin–orbit state. Also, the singlet states have the lowest and the highest energies, while all four triplet $(^3A)'$ states lie in between. The lowest $(^1A)'$ PES evidently correlates with the ground state of the $CSCl_2$ molecule. It is seen from Fig. 5 that the only $(^1A)''$ state adiabatically correlates with the upper spin–orbit state of the Cl atom having the largest energy, while all five $(^3A)''$ states lie below.

The PES of $(A)'$ and $(A)''$ symmetry related to the $Cl + R(\pi)$ channel obtained by diagonalisation of the corresponding 12×12 Hamiltonian matrices are shown in Figs. 6 and 7. This dissociation channel leads to population of the $\tilde{A}$ quantum state of the molecular fragment [14]. There are six singlet molecular states correlating with the $Cl + R(\pi)$ fragments: three of them are of $(^1A)'$ symmetry and three of $(^1A)''$ symmetry. It is easy to see from Fig. 6 that two of the singlet $(^1A)'$ states adiabatically correlate with the lower spin–orbit state of the Cl atom, while the third $(^1A)'$ state correlates with the upper spin–orbit state. In case of the $(A)''$ states in Fig. 7

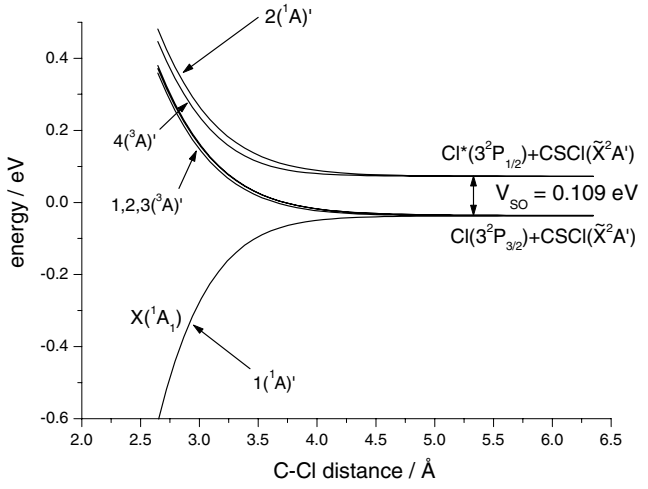

Fig. 4. Long-range PES for $Cl(^2P_j) + CSCl(^2\sigma)$: $(A)'$ symmetry states. The PES are shown for the $Cl + CSCl(\tilde{X})$ product channel. The situation is identical for the $Cl + CSCl(\tilde{B})$ product channel (not shown here).

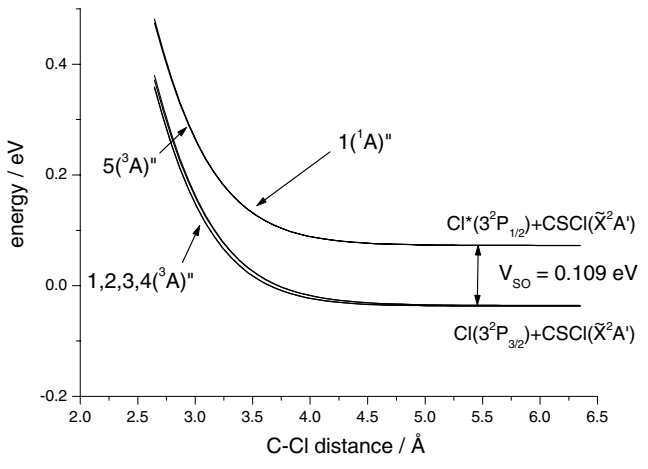

Fig. 5. Long-range PES for $Cl(^2P_j) + CSCl(^2\sigma)$: $(A)''$ symmetry states. The PES are shown for the $Cl + CSCl(\tilde{X})$ product channel. The situation is identical for the $Cl + CSCl(\tilde{B})$ product channel (not shown here).

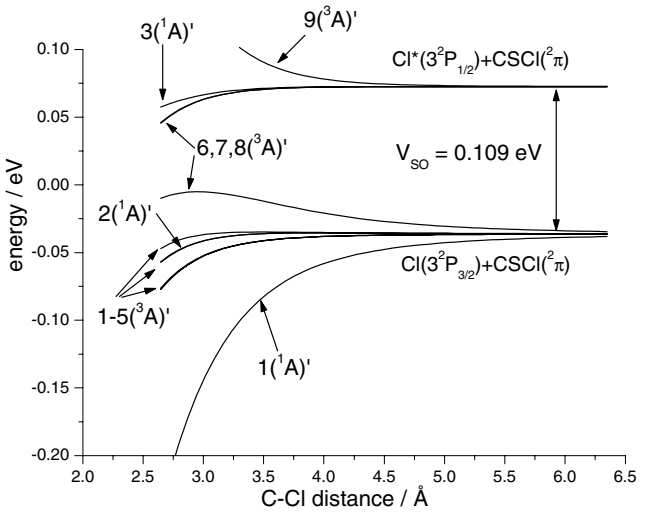

Fig. 6. Long-range potential energy curves for $Cl(^2P_j) + CSCl(^2\pi)$: $(A)'$ symmetry states, applicable to the $Cl + CSCl(\tilde{A})$ product channel.

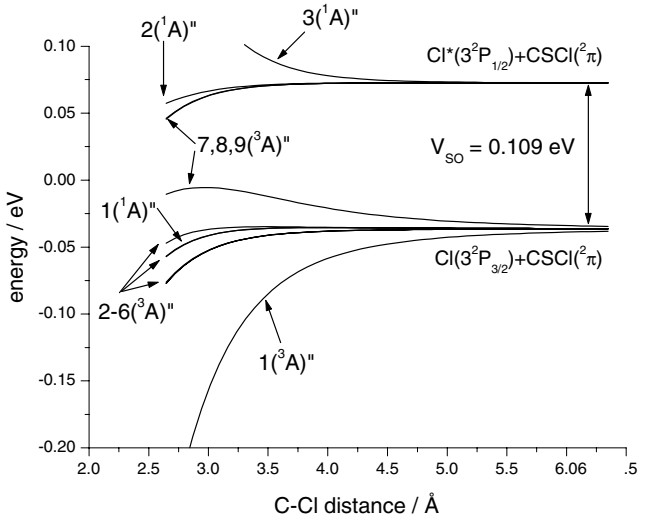

Fig. 7. Long-range potential energy curves for $Cl(^2P_j) + CSCl(^2\pi)$: $(A)''$ symmetry states, applicable to the $Cl + CSCl(\tilde{A})$ product channel.

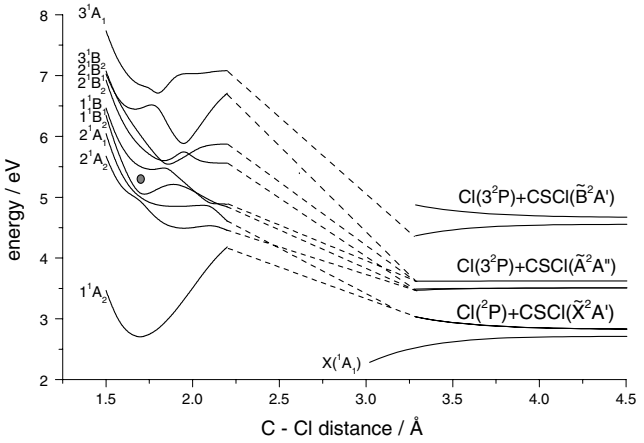

Fig. 8. Correlation diagram for $Cl(^2P_j) + CSCl$ photodissociation of thiophosgene: singlet states. The shaded circle marks the Franck–Condon region for 235-nm excitation.

two of the singlet $(^1A)''$ states adiabatically correlate with the upper spin–orbit state of Cl atom and the third $(^1A)''$ state correlates with the lower spin–orbit state.

4.2.3. Composite PES

The composite PES, including the results of both short-range and long-range calculations, are shown in Fig. 8. Only the singlet states of $^1A'$ and $^1A''$ symmetry are shown in this figure, because optical excitation to the triplet states is much less intensive in the $CSCl_2$ case. The excited PES in the SPS region are presented for R values from 1.5 to 2.2 Å and those in the WPS–FFS region are presented for R values from 3.3 to 4.5 Å, including the ground state surface which is not shown in the SPS region. In the intermediate range (2.2 Å $\leqslant R \leqslant$ 3.3 Å), where both calculation methods we used are not reliable enough, the potential curves from the SPS region are connected with those in the WPS–FFS region with straight dashed lines using the non-crossing rule of the potential curves of the same symmetry.

5. Discussion: fragment spin–orbit branching ratio and kinetic energy distribution

We assume that the spin–orbit interaction is not important at small and intermediate recoil distances R and consider the manifold of the singlet PES shown in Fig. 8.

As shown in Fig. 8, the following excited states of the parent molecule can be excited optically by 235 nm UV photons: 2^1A_2, 2^1A_1, 1^1B_2, 1^1B_1, and 2^1B_2. Although the oscillator strength for the 2^1A_1 excited state is much larger than that for other excited states (see Table 1), the nontrivial shape of the absorption profile in the vicinity of 235 nm excitation wavelength in Fig. 3 indicates that photodissociation of thiophosgene can occur via several different excited states. Optical excitation from the parent molecule ground state X^1A_1 to the 2^1A_2 excited state is dipole-forbidden within the framework of C_{2v} symmetry and according to our calculations (see Tables 2 and 3) it is negligible also in the non-equilibrium geometries. Although this is not the focus of the present work this state might also play a role in the discussion about the dark state associated with the 1^1B_2 state. Two of the remaining four states, 2^1A_1 and 1^1B_2, have $^1A'$ symmetry and according to the data in Table 1 they can be excited optically from the equilibrium ground state molecular geometry. They are to be identified as the B^1A_1 and the C^1B_2 states in the CASSCF calculations of Gruebele and coworkers [18]. According to our calculation the third state 1^1B_1 has $^1A''$ symmetry and will mainly be excited from non-equilibrium ground state geometry only (see Table 2). Analysis of the experimentally determined β parameter does not allow to unambiguously establish the upper excited state: the reported small positive value of β[7] can be explained either by population of the 2^1A_1 state only [13], or by simultaneous population of the1^1B_1 state together with the 1^1B_2 or the 2^1B_2 state with roughly equal intensities. We prefer the latter possibility because previous studies have proven that the $2^1A_1 \leftarrow X^1A_1$ transition is associated with the structured long wavelength wing of the strong absorption feature peaking at 250 nm. Also, the effect of the huge difference in the calculated oscillator strengths for the 2^1A_1 and 1^1B_2, 1^1B_1 quantum states in Table 1 can be reduced by taking into account the corresponding Franck–Condon factors. Fig. 8 shows that the 2^1A_1, 1^1B_2, and 1^1B_1 excited states adiabatically correlate with the $Cl^*(^2P_{1/2}) + R(\tilde{X})$, $Cl(^2P_{3/2}) + R(\tilde{A})$, and $Cl^*(^2P_{1/2}) + R(\tilde{A})$ fragments, respectively. Therefore, population of other multiple fragment states reported in experiment [7] must be due to non-adiabatic interaction and non-planarity in the molecular excited state.

A possible mechanism for the non-planarity can be the out-of-plane vibration of the excited molecule which mixes states of A'' and A' symmetry. Non-adiabatic interaction mechanisms resulting in mixing states of the same symmetry are also possible. In order to estimate the probability of the non-adiabatic transitions between different spin–orbit states in the *long range*, we calculated the Massey parameter [33] as

$$\eta = \frac{\Delta R \cdot V_{SO}}{v\hbar} \geqslant 6, \tag{11}$$

where ΔR is a characteristic interaction distance ($\Delta R \approx 1$ Å), V_{SO} is the spin–orbit interaction in the Cl fragment ($V_{SO} = 0.109$ eV), and v is the relative fragment speed ($v \approx 3000$ m/s).

A large value of the Massey parameter η in Eq. (11) manifests that the probability of the non-adiabatic transitions is small, that is the molecular system behaves almost adiabatically at large recoil distances R. Therefore, the non-adiabatic transitions and non-planarity between different molecular states occur mainly at *small*

and *intermediate* recoil distances. The probability of these transitions can be determined within the solution of the complex dynamic photodissociation problem using multidimensional PES which are not available now. However, some important conclusions about the dissociation process can be obtained by considering the one-dimensional PES in Fig. 8. Below, we discuss each dissociation channel separately.

In the following paragraphs the C_s notation always refers to the wavefunctions in the WPS–FFS region as shown in Figs. 4–7, while C_{2v} notation always refers to the parent molecule wavefunction in the SPS region. In case of the energetically lowest $Cl(^2P_j) + CSCl(\tilde{X})$ dissociation channel which produces fast chlorine photofragments the singlet $1(^1A)'$ state resulting in the $Cl(^2P_{3/2})$ fragments correlates with the parent molecule ground state X^1A_1 (see Figs. 4, 5 and 8). We assume that this singlet state can be populated only weakly in photodissociation through the non-adiabatic transitions and that the $Cl(^2P_j) + CSCl(\tilde{X})$ channel is mainly populated via two other singlet states, $2(^1A)'$ and $1(^1A)''$, giving the spin–orbit excited $Cl^*(^2P_{1/2})$ atoms. One of them, the $2(^1A)'$ state, can be directly populated via the $CSCl_2(3^1A_1) \leftarrow CSCl_2(X^1A_1)$ optical excitation, while the other one can be populated only indirectly, by non-adiabatic interaction and non-planarity. Therefore, we come to the conclusion that the photodissociation resulting in ground state molecular fragments $CSCl(\tilde{X})$ produces chlorine atoms predominantly in their upper $^2P_{1/2}$ spin–orbit state.

The energetically highest $Cl(^2P_j) + CSCl(\tilde{B})$ dissociation channel producing slow chlorine photofragments can also be treated with Figs. 4 and 5, if the $CSCl(\tilde{X})$ product state is replaced by $CSCl(\tilde{B})$. In this case, however, all three singlet states can be populated only indirectly by non-adiabatic and non-planarity interaction. The lowest $(^1A)'$ state giving the ground state $Cl(^2P_{3/2})$ fragments can have the major contribution to the photoprocess, as two other singlet states lie too high and are unlikely to be populated effectively. Therefore, the photodissociation channel resulting in the excited state fragments $CSCl(\tilde{B})$ produces chlorine atoms predominantly in their lower spin–orbit state $^2P_{3/2}$. Both the above conclusions are in qualitative agreement with the experimental result in Fig. 2.

Interpretation of the intermediate energy $Cl(^2P_j) + CSCl(\tilde{A})$ channel is more complicated because in total there are as many as six singlet states which can be populated either directly or by non-adiabatic interactions and non-planarity (see Figs. 6 and 7). According to the correlation diagram in Fig. 8 the 2^1A_2, 1^1B_2, and 2^1B_2 states correlate adiabatically with the Cl channel, while the 1^1B_1, 3^1B_2, and 2^1B_1 states correlate with the Cl^* channel. Each of the lower and upper chlorine spin–orbit state can directly be populated optically via the 1^1B_2 and the 1^1B_1 molecular quantum states, respectively. Assuming approximately the same population of both three-level manifolds above, we come to the conclusion that the intermediate kinetic energy Cl and Cl^* atoms which are produced in this channel have approximately the same concentration in agreement with the experimental data in Fig. 2.

Table 6
Relative population of the $CSCl_2$ quantum states in photodissociation

Molecular energy level groups	Relative population
X^1A_1	2
$2^1A_1 + 1^1A_2$	3.5
$2^1A_2 + 1^1B_2 + 2^1B_2$	32
$1^1B_1 + 2^1B_1 + 3^1B_2$	33
3^1A_1	19
?	10

The group of high-lying states indicated by (?) have not been calculated in this work.

Having in mind almost adiabatic behaviour of the molecular system at large internuclear distances, one comes to the important conclusion that the branching ratios of the Cl and Cl^* atoms corresponding to different states of the CSCl fragment contain direct information about the relative population of the molecular states in the SPS region by photons and following non-adiabatic transitions and non-planarity. These relative populations which were obtained using the correlation diagram in Fig. 8 and the experimental branching ratios given above in Section 2 are presented in Table 6.

6. Conclusion

A theoretical approach has been developed for the interpretation of the kinetic energy-dependent spin–orbit state distributions of chlorine photofragments produced in the photodissociation of a polyatomic chlorine-containing molecule. The approach was used in the case of thiophosgene dissociation at 235 nm. It is based on the computation of the $CSCl_2$ PES along the C–Cl bond using the basis molecular wavefunctions with definite multiplicity and spatial and spin reflection symmetry σ_v. The theory predicts almost adiabatic dissociation of the parent molecule at large recoil distances and strong dependence of the spin–orbit state branching ratio of the chlorine atoms on the quantum state of the CSCl partner fragment. The developed theoretical model is general and can be used for the interpretation of results in other polyatomic molecules containing chlorine atoms.

Acknowledgements

We are grateful to George Maroulis for calculating the quadrupole moments of the CSCl molecule and for useful discussions. These studies were supported by the Alexander von Humboldt Foundation and by the Russian Foundation for Basic Researches, Grant # 02-03-32914.

References

[1] H. Okabe, Photochemistry of Small Molecules, Wiley-Interscience, New York, 1978.
[2] Y. Matsumi, K. Tonokura, M. Kawasaki, G. Inoue, S. Satyapal, R. Bersohn, J. Chem. Phys. 94 (1991) 2669.
[3] S. Satyapal, S. Tasaki, R. Bersohn, Chem. Phys. Lett. 203 (1993) 349.
[4] C. Maul, T. Haas, K.-H. Gericke, F.J. Comes, J. Chem. Phys. 102 (1995) 3238.
[5] M. Kawasaki, K. Suto, Y. Sato, Y. Matsumi, R. Bersohn, J. Phys. Chem. 100 (1996) 19853.
[6] T. Einfeld, A. Chichinin, C. Maul, K.-H. Gericke, J. Chem. Phys. 116 (2002) 2803.
[7] T. Einfeld, A. Chichinin, C. Maul, K.-H. Gericke, J. Chem. Phys. 117 (2002) 1123.
[8] R.S. Mulliken, Phys. Rev. 50 (1936) 1017;
R.S. Mulliken, J. Chem. Phys. 8 (1950) 382.
[9] A. Maciejewski, R.P. Steer, Chem. Rev. 93 (1993) 67, and references therein.
[10] E.R. Farnworth, G.W. King, J. Mol. Spectrosc. 46 (1973) 419.
[11] H. Okabe, J. Chem. Phys. 66 (1977) 2058.
[12] B. Simard, A.E. Bruno, P.G. Mezey, R.P. Steer, Chem. Phys. 103 (1986) 75.
[13] G.S. Ondrey, R. Bersohn, J. Chem. Phys. 79 (1983) 175.
[14] M. Hachey, F. Green, R.P. Steer, Can. J. Chem. 71 (1993) 112.
[15] J.H. Carpenter, D.F. Rimmer, J.G. Smith, D.H. Whiffen, J. Chem. Soc., Faraday Trans. 2 71 (1975) 1752.
[16] D. Chadwick, Can. J. Chem. 50 (1972) 737.
[17] R. Bigwood, B. Milam, M. Gruebele, Chem. Phys. Lett. 287 (1998) 333.
[18] T. Fujiwara, E.C. Lin, D.C. Moule, J. Chem. Phys. 119 (2003) 7741;
A.M. Warsylewicz, K.J. Falk, R.P. Steer, Chem. Phys. Lett. 352 (2002) 48;
B. Strickler, M. Gruebele, Chem. Phys. Lett. 349 (2001) 137;
B. Simard, V.J. MacKenzie, P.A. Hackett, R.P. Steer, Can. J. Chem. 72 (1994) 745;
M. Ludwiczak, D.R. Latimer, R.P. Steer, J. Mol. Spectrosc. 147 (1991) 414;
R.N. Dixon, C.M. Western, J. Mol. Spectrosc. 115 (1986) 74;
R.H. Judge, D.C. Moule, J. Mol. Spectrosc. 80 (1980) 363.
[19] S.Z. Levine, A.R. Knight, R.P. Steer, Chem. Phys. Lett. 29 (1974) 73.
[20] A. Chichinin, T. Einfeld, K.-H. Gericke, C. Maul, in: B. Whitaker (Ed.), Imaging in Molecular Dynamics: Technology and Applications, Cambridge University Press, Cambridge, 2003.
[21] A. Chichinin, T. Einfeld, C. Maul, K.-H. Gericke, Rev. Sci. Instrum. 73 (2002) 1856.
[22] E.U.K. Gross, J.F. Dobson, M. Petersilka, in: R.F. Nalewajski (Ed.), Density Functional Theory II, Springer Series in Topics in Current Chemistry, Springer, Heidelberg, 1996.
[23] A.D. Becke, J. Chem. Phys. 98 (1993) 5648.
[24] M.J. Frisch, G.W. Trucks, H.B. Schlegel, G.E. Scuseria, M.A. Robb, J.R. Cheeseman, V.G. Zakrzewski, J.A. Montgomery Jr., R.E. Stratmann, J.C. Burant, S. Dapprich, J.M. Millam, A.D. Daniels, K.N. Kudin, M.C. Strain, O. Farkas, J. Tomasi, V. Barone, M. Cossi, R. Cammi, B. Mennucci, C. Pomelli, C. Adamo, S. Clifford, J. Ochterski, G.A. Petersson, P.Y. Ayala, Q. Cui, K. Morokuma, P. Salvador, J.J. Dannenberg, D.K. Malick, A.D. Rabuck, K. Raghavachari, J.B. Foresman, J. Cioslowski, J.V. Ortiz, A.G. Baboul, B.B. Stefanov, G. Lui, A. Liashenko, P. Piskorz, I. Komaromi, R. Gomperts, R.L. Martin, D.J. Fox, T. Keith, M.A. Al-Laham, C.Y. Peng, A. Nanayakkara, M. Challacombe, P.M.W. Gill, B. Johnson, W. Chen, M.W. Wong, J.L. Andres, C. Gonzales, M. Head-Gordon, E.S. Replogle, J.A. Pople, Gaussian 98, Rev. A.11.1, Gaussian Inc., Pittsburgh, PA, 2001.
[25] M. Casida, C. Jamorski, K. Casida, D. Salahub, J. Chem. Phys. 108 (1998) 4439.
[26] E.E. Nikitin, J. Troe, J. Chem. Phys. 92 (1990) 6594.
[27] O.S. Vasyutinskii, P.S. Shternin, E.V. Orlenko, in preparation.
[28] C.G. Gray, Can. J. Phys. 46 (1968) 135.
[29] E.V. Orlenko, A.A. Rumyantsev, Sov. Phys. JETP 70 (1990) 244.
[30] A.V. Evseev, A.A. Radzig, B.M. Smirnov, Opt. Spektrosc. 44 (1978) 883.
[31] D.A. Varshalovich, A.N. Moskalev, V.K. Khersonskii, Quantum Theory of Angular Momentum, World Scientific, Singapore, 1988.
[32] I.I. Sobelman, Atomic Spectra and Radiative Transitions, Springer, Berlin, Heidelberg, New York, 1979.
[33] N.F. Mott, H.S.W. Massey, The Theory of Atomic Collisions, Clarendon Press, Oxford, 1965.